# NEW SOLITARY WAVE STRUCTURES IN TWO-DIMENSIONAL PERIODIC MEDIA

ZUOQIANG SHI* AND JIANKE YANG†
*Zhou Pei-Yuan Center for Applied Mathematics*
*Tsinghua University*
*Beijing, China, 100084*

New solitary-wave structures in two-dimensional periodic media are obtained in the context of a two-dimensional nonlinear Schrödinger equation with a periodic potential. These new structures bifurcate from the edges of Bloch bands with two linearly independent Bloch modes. Away from these band edges, superposition of these Bloch modes, modulated by nonlinear effects, give rise to composite solitary waves with distinctive intensity and phase profiles such as vortex arrays. Using perturbation methods, coupled nonlinear envelope equations for the two Bloch waves near the band edges are analytically derived. Numerically, these composite solitons are directly computed both near and far away from the band edges, and the analytical results are fully confirmed.

## 1. Introduction

Nonlinear wave propagation in periodic media is attracting a lot of attention these days. This was stimulated in part by rapid advances in optics, Bose-Einstein condensation, and related fields. In optics, various periodic and quasi-periodic structures (such as photonic crystals, photonic crystal fibers, periodic waveguide arrays and photonic lattices) have been constructed by ingeneous experimental techniques, with applications to light routing, switching and optical information processing [1,2,3,4,5,6]. This periodic medium creates a wide range of new phenomena for light propagation, even in the linear regime. For instance, the diffraction of light in a periodic medium exhibits distinctively different patterns from homogeneous diffraction [3]. If the periodic medium has a local defect, this defect can guide light by a totally new physical mechanism called repeated Bragg reflections [2,7,8]. When the nonlinear effects become significant, say with high-power beams or in strongly nonlinear materials such as photorefractive crystals, the physical phenomena would be even richer and more complex, and their understanding is far from complete yet. In Bose-Einstein condensates, one direction of recent research is to load these condensates into periodic optical lattices [9]. This problem and the above nonlinear optics problems are closely

*email: shizq03@mails.tsinghua.edu.cn
†Permanent address: Department of Mathematics and Statistics, University of Vermont, Burlington, VT 05401, USA; email: jyang@math.uvm.edu.

related, and are often analyzed together in the mathematical community.

Solitary waves play an important role in nonlinear wave systems. These waves are nonlinear localized structures which propagate without change of shape. In physical communities, they are often just called solitons, which we do occasionally in this paper as well. If a physical system admits solitary waves, it often has important consequences. For instance, optical fibers can support solitary waves (pulses) when the nonlinearity of the pulse balances linear dispersion. This fact led to soliton-based fiber communication systems, which greatly propelled the telecommunication industry in the end of the last century. In one-dimensional periodic media, solitary waves (called lattice solitons) also exist, and they have been observed in optical experiments [3,10,11,12]. But two- (or higher-) dimensional periodic media can support a much wider array of solitary wave structures which have no counterpart in one-dimensional systems. One example is the vortex lattice solitons which was predicted in [13,14] and later observed in [15,16]. These vortex solitons lie in the semi-infinite bandgap of the periodic system. Recently, Bartal, et al. [17] reported the observation of vortex solitons which lie in a higher bandgap of a periodic medium, and Makazyuk, et al. [18] reported the observation of linear localized light patterns which comprise of dipole or vortex-cell arrays in a defected 2D lattice. Even though these two observations are quite different, their common feature is that Bloch-wave superpositions were essential for their explanations. These observations indicate that Bloch-wave superpositions can create novel and intricate solitary-wave patterns. However, it is not clear at the moment what are all the possible solitary-wave structures this Bloch-wave superposition can create, and which edges of Bloch bands these structures can bifurcate from. In-depth analytical studies on these new structures are totally missing as well.

In this paper, we analyze all possible solitary-wave structures due to Bloch-wave superpositions in two-dimensional periodic media both analytically and numerically, using the two-dimensional nonlinear Schrödinger equation with a periodic potential as the mathematical model. First, we identify edges of Bloch bands which admit two linearly independent Bloch modes. Then using perturbation methods, we derive coupled nonlinear equations for envelopes of these superposing Bloch waves near these band edges. We find that these envelope equations admit solutions which lead to novel solitary-wave structures such as vortex-array solitons if the nonlinearity is of the same sign as the second-order dispersion coefficients of Bloch waves on the underlying band edges. Hence these composite solitons exist for both focusing and defocusing nonlinearities. We have also computed these composite solitons directly by numerical methods both near and further away from the band edges. In the former case, the numerical results are in full agreement with the analytical calculations.

## 2. The Mathematical Model

The mathematical model for the study of solitary waves in periodic media is the two-dimensional (2D) nonlinear Schr"odinger (NLS) equation with a periodic potential:

$$iU_t + U_{xx} + U_{yy} - V(x,y)U + \sigma|U|^2U = 0, \tag{1}$$

where $V(x,y)$ is the periodic potential, and $\sigma = \pm 1$ is the sign of nonlinearity. This model naturally arises for light propagation in a periodic Kerr medium, and for Bose-Einstein condensates trapped in an optical lattice [9]. In certain optical materials (such as photorefractive crystals), the nonlinearity is of a different (saturable) type. But it is known that these different types of nonlinearities give qualitatively similar results [14,15,16,19].

In this article we take the periodic potential as

$$V(x,y) = V_0\left(\sin^2 x + \sin^2 y\right), \tag{2}$$

whose periods along the $x$ and $y$ directions are both equal to $\pi$. This potential is separable, which facilitates our theoretical analysis. In addition, without loss of generality, when specific computations are carried out, we always set $V_0 = 6$.

Solitary waves in Eq. (1) are sought in the form

$$U(x,y,t) = u(x,y)e^{-i\mu t}, \tag{3}$$

where amplitude function $u(x,y)$ is a solution of the following equation:

$$u_{xx} + u_{yy} - [F(x) + F(y)]u + \mu u + \sigma|u|^2u = 0, \tag{4}$$

$$F(x) = V_0 \sin^2 x, \tag{5}$$

and $\mu$ is a propagation constant.

## 3. Bloch bands and band gaps

When function $u(x,y)$ is infinitesimal, Eq. (4) becomes a linear equation:

$$u_{xx} + u_{yy} - [F(x) + F(y)]u + \mu u = 0. \tag{6}$$

Solutions of this linear equation are the Bloch modes, and the corresponding propagation constants $\mu$ form Bloch bands. Since the potential in (6) is separable, Bloch solutions and Bloch bands of the 2D equation (6) can be obtained from solutions of a 1D equation. Specifically, the 2D Bloch solution $u(x,y)$ of Eq. (6) and the propagation constant $\mu$ can be split into the following form:

$$u(x,y) = p(x;\omega_a)p(y;\omega_b), \quad \mu = \omega_a + \omega_b, \tag{7}$$

where $p(x;\omega)$ is a solution of the following 1D equation:

$$p_{xx} - F(x)p + \omega p = 0. \tag{8}$$

Eq. (8) is equivalent to the Mathieu equation. Its solution is

$$p(x;\omega) = e^{ikx}\tilde{p}(x;\omega), \tag{9}$$

where $\tilde{p}(x;\omega)$ is periodic with period $\pi$, and

$$\omega = \omega(k) \tag{10}$$

is the 1D dispersion relation. This dispersion diagram is shown in Fig. 1(a) (for $V_0 = 6$). The bandgap structure at various values of $V_0$ are shown in Fig. 1(b). The four Bloch waves at both edges of the lowest two Bloch bands are displayed in Fig. 2.

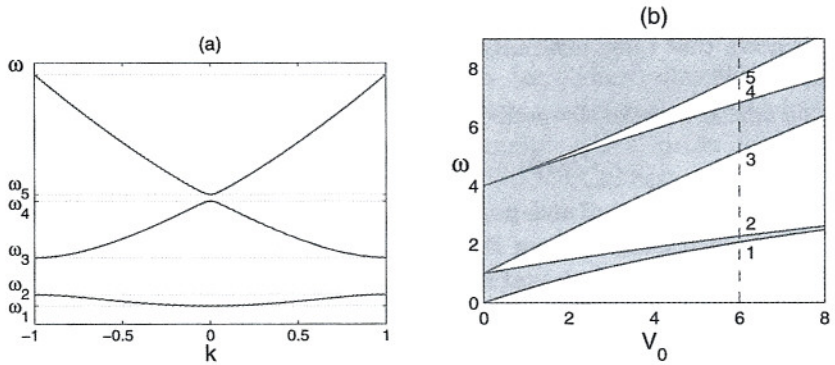


Figure 1. (a) Dispersion curves of the 1D equation (8) with $V_0 = 6$; (b) Bloch bands (shaded regions) and bandgaps at various values of potential levels $V_0$ in the 1D equation (8).

Using these 1D dispersion results and the above connection between 1D and 2D Bloch solutions, we can construct the dispersion surfaces and band gap structures for the 2D problem (6), and the results are shown in Fig. 3. In Fig. 3 (a), the dispersion surfaces of the 2D problem are displayed at $V_0 = 6$. The 2D bandgap structure at various values of $V_0$ are shown in Fig. 3 (b). Unlike the 1D case, for a given $V_0$ value, there are only a finite number of bandgaps in the 2D problem. The first bandgap appears only when $V_0 > 1.40$, the second bandgap appearing when $V_0 > 4.13$, etc. As $V_0$ increases further, more bandgaps will be found.

Now we examine the 2D Bloch solutions on the edges of Bloch bands. To illustrate, we consider the points A, B, C, D and E marked in Fig. 3 (b), where $V_0 = 6$. At each of points A and B, there is a *single* Bloch solution, which is symmetric along the $x$ and $y$ directions, i.e., $u(x,y) = u(y,x)$. In view of the relation (7), it is easy to see that the Bloch solution at point A is $p(x;\omega_1)p(y;\omega_1)$, where $\omega_1$ marked in Fig. 1(a), and $p(x;\omega_2)$ is shown in Fig. 2(a). For convenience, we denote point A as "1 + 1". Similarly, the 2D Bloch solution at point B is $p(x;\omega_2)p(y;\omega_2)$, where $\omega_2$ marked in Fig. 1(a), and $p(x;\omega_2)$ is shown in Fig. 2(b). Point B is 2+2 in our notations. Points C, D, E are different from A and B and are much more interesting, however. At these points, there are *two* linearly independent Bloch solutions, $u(x,y)$ and $u(y,x)$. For instance, at point C, these two solutions are $p(x;\omega_1)p(y;\omega_3)$ and $p(y;\omega_1)p(x;\omega_3)$, where $\omega_3$ is marked in Fig. 1(a), and $p(x;\omega_3)$

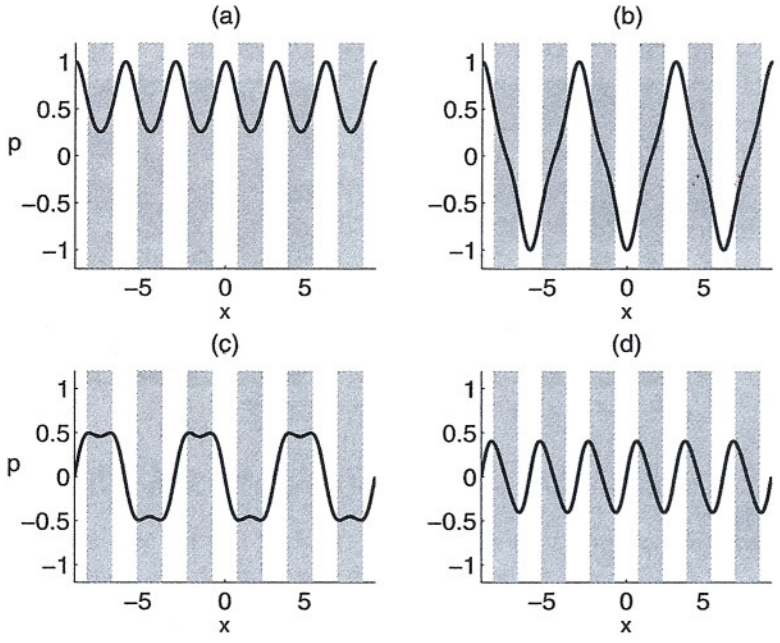


Figure 2. The first four 1D Bloch waves at edges of Bloch bands marked by letters $\omega_1, \omega_2, \omega_3$ and $\omega_4$ in Fig. 1(a). (a): $\omega_1 = 2.063182$; (b): $\omega_2 = 2.266735$; (c): $\omega_3 = 5.165940$; (d): $\omega_4 = 6.81429$.

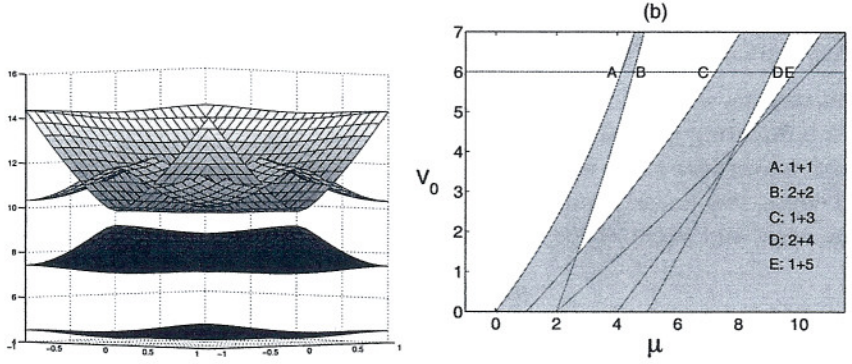


Figure 3. (a) Dispersion surfaces of the 2D problem (6) at $V_0 = 6$; (b) the 2D bandgap structure for various values of $V_0$.

is shown in Fig. 2(c). Point C is "1+3". The solution $p(x;\omega_1)p(y;\omega_3)$ is displayed in Fig. 4(a). Point D is "2+4", where the two linearly independent Bloch solutions are $p(x;\omega_2)p(y;\omega_4)$ and $p(y;\omega_2)p(x;\omega_4)$, the former of which is displayed in Fig. 4(b). Point E is "1+5". Because of the existence of two linearly independent Bloch solutions, their linear superposition remains a solution. These superpositions can give rise to interesting composite patterns such as vortex arrays, as has been pointed

out in [17,18].

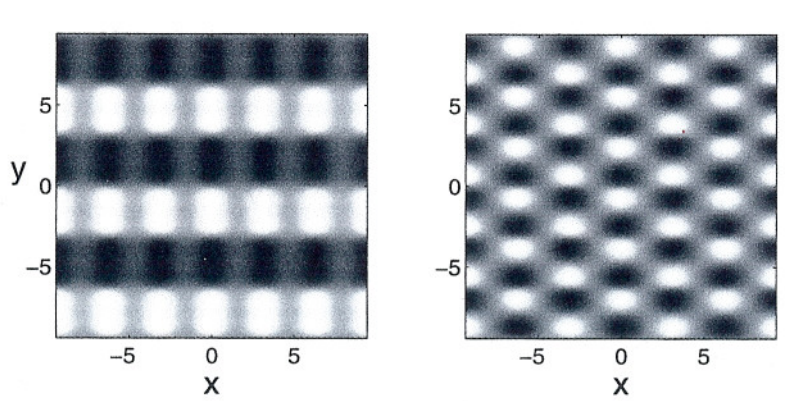


Figure 4. (a) A 2D Bloch mode at point C marked in Fig. 3; (b) A 2D Bloch mode at point D marked in Fig. 3.

The above superposing Bloch solutions exist on band edges with infinitesimal amplitudes. When amplitudes of these solutions increase, these Bloch solutions may localize and form solitary-wave structures. These solitary waves exist not on band edges, but inside bandgaps. In the next section, we analyze these solutions by perturbation methods in the limit when these solutions lie near the Bloch bands.

## 4. Asymptotic derivation of coupled envelope equations

In this section, we develop an asymptotic theory to analyze small-amplitude solitary waves bifurcating from superimposing Bloch waves near band edges in Eq. (4).

Let us consider a 2D band edge $\mu_0 = \omega_{0,1} + \omega_{0,2}$, where $\omega_{0,n}$ $(n = 1, 2)$ are 1D band edges, two linearly independent Bloch modes $p_1(x)p_2(y)$ and $p_1(y)p_2(x)$ exist at the edge, and $p_n(x) = p(x; \omega_{0,n})$ $(n = 1, 2)$. Notice that

$$p_n(x + L) = \pm p_n(x) \tag{11}$$

since $\omega_{0,n}$ is a 1D band edge, and $L = \pi$ is the period of the potential $F(x)$. We take an infinitesimal solution $u(x, y)$ of Eq. (4) which is a linear superposition of these two Bloch modes. When $u(x, y)$ is small but not infinitesimal, we can expand the solution $u(x, y)$ of Eq. (4) into a multi-scale perturbation series:

$$u = \epsilon u_0 + \epsilon^2 u_1 + \epsilon^3 u_2 + \cdots, \tag{12}$$

$$\mu = \mu_0 + \eta\epsilon^2, \tag{13}$$

where

$$u_0 = A_1(X, Y)p_1(x)p_2(y) + A_2(X, Y)p_2(x)p_1(y), \tag{14}$$

$\eta = \pm 1$, and $X = \epsilon x, Y = \epsilon y$. Substituting the above expansions into Eq. (4), the equation at $O(\epsilon)$ is automatically satisfied. At order $O(\epsilon^2)$, the equation is

$$u_{1xx} + u_{1yy} - (F(x) + F(y))u_1 + \mu_0 u_1 = -2\left(\frac{\partial^2 u_0}{\partial x \partial X} + \frac{\partial^2 u_0}{\partial y \partial Y}\right). \tag{15}$$

Its homogeneous equation has two linearly independent solutions, $p_1(x)p_2(y)$, and $p_1(y)p_2(x)$. In order for the inhomogeneous equation (15) to admit a solution, the following Fredholm conditions

$$\int_0^{2L}\int_0^{2L}\left(\frac{\partial^2 u_0}{\partial x \partial X} + \frac{\partial^2 u_0}{\partial y \partial Y}\right) p_1(x)p_2(y)\, dxdy = 0, \tag{16}$$

$$\int_0^{2L}\int_0^{2L}\left(\frac{\partial^2 u_0}{\partial x \partial X} + \frac{\partial^2 u_0}{\partial y \partial Y}\right) p_2(x)p_1(y)\, dxdy = 0, \tag{17}$$

must be satisfied. Here the integration length is $2L$ rather than $L$ since the homogeneous solutions $p_1(x)p_2(y)$ and $p_2(x)p_1(y)$ may have periods $2L$ along the $x$ and $y$ direction (see Eq. (11)). It is easy to check that these conditions are indeed satisfied automatically, thus we can find a solution for Eq. (15) as

$$u_1 = \frac{\partial A_1}{\partial X}\nu_1(x)p_2(y) + \frac{\partial A_1}{\partial X}\nu_2(y)p_1(x) + \frac{\partial A_2}{\partial X}\nu_2(x)p_1(y) + \frac{\partial A_2}{\partial X}\nu_1(y)p_2(x), \tag{18}$$

where $\nu_n(x)$ is a periodic solution of equation

$$\nu_{n,xx} - F(x)\nu_n + \omega_{0,n}\nu_n = -2p_{n,x}, \quad n = 1, 2. \tag{19}$$

At $O(\epsilon^3)$, the equation is

$$\begin{aligned} &u_{2xx} + u_{2yy} - (F(x) + F(y))u_2 + \mu_0 u_2 = \\ &\quad -\left(2\frac{\partial^2 u_1}{\partial x \partial X} + 2\frac{\partial^2 u_1}{\partial y \partial Y} + \frac{\partial^2 u_0}{\partial X^2} + \frac{\partial^2 u_0}{\partial Y^2} + \eta u_0 + |u_0|^2 u_0\right). \end{aligned} \tag{20}$$

Substituting the expressions for $u_0$ and $u_1$ into this equation, we get

$$\begin{aligned} &-[u_{2xx} + u_{2yy} - (F(x) + F(y))u_2 + \mu_0 u_2] = \\ &\frac{\partial^2 A_1}{\partial X^2}\left(2\frac{\nu_1(x)}{\partial x} + p_1(x)\right)p_2(y) + \frac{\partial^2 A_1}{\partial Y^2}\left(2\frac{\nu_2(y)}{\partial y} + p_2(y)\right)p_1(x) + \\ &\frac{\partial^2 A_2}{\partial X^2}\left(2\frac{\nu_2(x)}{\partial x} + p_2(x)\right)p_1(y) + \frac{\partial^2 A_2}{\partial Y^2}\left(2\frac{\nu_1(y)}{\partial y} + p_1(y)\right)p_2(x) + \\ &2\frac{\partial^2 A_1}{\partial X \partial Y}\left(\frac{\partial p_1(x)}{\partial x}\nu_2(y) + \frac{\partial p_2(y)}{\partial y}\nu_1(x)\right) + 2\frac{\partial^2 A_2}{\partial X \partial Y}\left(\frac{\partial p_2(x)}{\partial x}\nu_1(y) + \frac{\partial p_1(y)}{\partial y}\nu_2(x)\right) + \\ &p_1^3(x)p_2^3(y)|A_1|^2 A_1 + p_1(x)p_2(y)p_1^2(y)p_2^2(x)(\bar{A}_1 A_2^2 + 2A_1|A_2|^2) + \\ &p_2^3(x)p_1^3(y)|A_2|^2 A_2 + p_1^2(x)p_2^2(y)p_1(y)p_2(x)(\bar{A}_2 A_1^2 + 2A_2|A_1|^2) + \\ &\eta A_1(X, Y, T)p_1(x)p_2(y) + \eta A_2(X, Y, T)p_2(x)p_1(y). \end{aligned} \tag{21}$$

Here the overbar represents complex conjugation. Before applying the Fredholm conditions to this inhomogeneous equation, we notice the following identities:

$$\int_0^{2L} p_1(x)p_2(x)dx = 0, \tag{22}$$

$$\int_0^{2L} p_1(x)\nu_2(x)dx = \int_0^{2L} p_2(x)\nu_1(x)dx, \tag{23}$$

and

$$\int_0^{2L} \left(2\frac{\dot{\nu}_n(x)}{\partial x} + p_n(x)\right) p_n(x)dx = D_n \int_0^{2L} p_n^2(x)dx, \quad n = 1, 2, \tag{24}$$

where

$$D_n \equiv \frac{1}{2}\frac{d^2\omega}{dk^2}\bigg|_{\omega=\omega_{0,n}}. \tag{25}$$

Identity (22) holds since $p_1(x)$ and $p_2(x)$ are the eigenfunctions of the self-adjoint linear Schr"odinger operator with different eigenvalues. Identity (23) can be confirmed by taking the inner product between Eq. (19) and functions $p_n(x)$. Identity (24) can be verified by expanding the solution of Eq. (8) around the edge of the Bloch band $\omega = \omega_{0,n}$. Utilizing these identities and (11), the Fredholm conditions for Eq. (21) finally lead to the following coupled nonlinear equations for the envelope functions $A_1$ and $A_2$:

$$\begin{aligned} D_1\frac{\partial^2 A_1}{\partial X^2} + D_2\frac{\partial^2 A_1}{\partial Y^2} + \eta A_1 + \sigma\left[\alpha|A_1|^2A_1 + \beta\left(\bar{A}_1A_2^2 + 2A_1|A_2|^2\right)\right. \\ \left.+\gamma\left(|A_2|^2A_2 + \bar{A}_2A_1^2 + 2A_2|A_1|^2\right)\right] = 0, \end{aligned} \tag{26}$$

$$\begin{aligned} D_2\frac{\partial^2 A_2}{\partial X^2} + D_1\frac{\partial^2 A_2}{\partial Y^2} + \eta A_2 + \sigma\left[\alpha|A_2|^2A_2 + \beta\left(\bar{A}_2A_1^2 + 2A_2|A_1|^2\right)\right. \\ \left.+\gamma\left(|A_1|^2A_1 + \bar{A}_1A_2^2 + 2A_1|A_2|^2\right)\right] = 0. \end{aligned} \tag{27}$$

Here

$$\alpha = \frac{\int_0^{2L}\int_0^{2L} p_1^4(x)p_2^4(y)\,dxdy}{\int_0^{2L}\int_0^{2L} p_1^2(x)p_2^2(y)\,dxdy}, \tag{28}$$

$$\beta = \frac{\int_0^{2L}\int_0^{2L} p_1^2(x)p_2^2(x)p_1^2(y)p_2^2(y)\,dxdy}{\int_0^{2L}\int_0^{2L} p_1^2(x)p_2^2(y)\,dxdy}, \tag{29}$$

and

$$\gamma = \frac{\int_0^{2L}\int_0^{2L} p_1^3(x)p_2(x)p_2^3(y)p_1(y)\,dxdy}{\int_0^{2L}\int_0^{2L} p_1^2(x)p_2^2(y)\,dxdy}. \tag{30}$$

Notice that $\alpha$ and $\beta$ are always positive, but $\gamma$ may be positive or negative.

The coefficients in Eqs. (26)-(27) can be readily determined from solutions of the 1D equation (8). In particular, at point C,

$$D_1 = 0.434845, \quad D_2 = 2.422196, \quad \alpha = 0.142814, \quad \beta = 0.032511, \quad \gamma = 0; \tag{31}$$

at point D,

$$D_1 = 0.586799, \quad D_2 = 13.264815, \quad \alpha = 0.086031, \quad \beta = 0.029655, \quad \gamma = 0; \tag{32}$$

and at point E,

$$D_1 = 0.434845, \; D_2 = 15.793172, \; \alpha = 0.971951, \; \beta = 0.162160, \; \gamma = -0.054081. \tag{33}$$

It is noted that near band edges where a single Bloch mode exists (such as points $A$ and $B$ in Fig. 3), the envelope equation for this single Bloch mode can be more easily derived. In this case, this single Bloch mode must be of the form $p(x;\omega_n)p(y;\omega_n)$, where $\omega_n$ is a band edge in the 1D problem (8). The resulting envelope equation for this Bloch mode is

$$D_1\left(\frac{\partial^2 A_1}{\partial X^2} + \frac{\partial^2 A_1}{\partial Y^2}\right) + \eta A_1 + \sigma\alpha_0|A_1|^2 A_1 = 0, \tag{34}$$

where

$$D_1 = \frac{1}{2}\frac{d^2\omega}{dk^2}\bigg|_{\omega=\omega_n}, \quad \alpha_0 = \frac{\int_0^{2L}\int_0^{2L} p_1^4(x)p_1^4(y)\,dxdy}{\int_0^{2L}\int_0^{2L} p_1^2(x)p_1^2(y)\,dxdy}, \tag{35}$$

and $p_1(x) = p(x;\omega_n)$.

From the above asymptotic solutions, we can calculate the power of the corresponding composite solitary wave as $\epsilon \to 0$ (i.e. on the band edge). Details will be omitted here.

## 5. Solutions of the coupled envelope equations

Envelope equations (26)-(27) are the key results of this article. They have important consequences. First, they show that solitary waves are possible only when $\eta D_1 < 0, \eta D_2 < 0$. In this case, $\mu$ lies in the bandgap of the linear system as expected (see Eq. (13). Second, they show that solitary waves exist only when the dispersion coefficients $D_1, D_2$ and the nonlinearity coefficient $\sigma$ are of the same sign. For instance, at point C in Fig. 3 where $D_1 > 0, D_2 > 0$, solitary waves exist only when

$\sigma > 0$, i.e., for focusing nonlinearity, not for defocusing nonlinearity. The situation is opposite at point $D$.

Below we study solutions of envelope equations (26)-(27). This system allows various reductions. If $\gamma = 0$, it allows the following three simple reductions:

(a) $A_1 > 0$, $A_2 = 0$, or $A_1 = 0, A_2 \neq 0$. In this case, the solution is a single Bloch-wave envelope solution.

(b) $A_1 > 0$, $A_2 > 0$. In this case, the solution is a composite real-valued envelope state. Note that the $A_1 > 0, A_2 < 0$ solution, or $A_1 < 0, A_2 > 0$ solution, or $A_1 < 0, A_2 < 0$ solution, or $A_1, A_2$ being both purely imaginary solution, is equivalent to the $A_1 > 0, A_2 > 0$ solution in (26)-(27), and leads to the equivalent solitary waves in the original system (4).

(c) $A_1 > 0$, $A_2 = i\hat{A}_2$, $\hat{A}_2 > 0$. In this case, the solution is a composite complex-valued envelope state. Note that other solutions of $A_1$ purely imaginary and $A_2$ real are equivalent to this real $A_1$ and purely imaginary $A_2$ solution.

If $\gamma \neq 0$, however, the reductions are quite different. For instance, the first and third reductions of case $\gamma = 0$ no longer hold. In this case, the following two reductions are allowed:

(a) $A_1 > 0$, $A_2 > 0$. In this case, the solution is a composite real-valued envelope state;

(b) $A_1 > 0, A_2 < 0$. In this case, the solution is another composite real-valued envelope state *different* from the $A_1 > 0$, $A_2 > 0$ reduction.

It is note-worthy that at band edges with $\gamma \neq 0$, the single Bloch-wave envelope reduction of $A_1 \neq 0$, $A_2 = 0$ or $A_1 = 0, A_2 \neq 0$ is not possible. Physically, this is due to a resonance between the two Bloch modes, which prevents the existence of a single Bloch mode envelope solution. For instance, at point $E$ in Fig. 3 where the two Bloch solutions are $p(x;\omega_1)p(y;\omega_5)$ and $p(y;\omega_1)p(x;\omega_5)$, both $p(x;\omega_1)$ and $p(x;\omega_5)$ are symmetric in $x$ and have period $\pi$. Thus these two modes are in resonance. At points where $\gamma = 0$ (such as point $C$ and $D$ in Fig. 3), the two Bloch solutions are not in resonance due to different symmetries, thus single Bloch-wave reduction is possible there.

To illustrate the composite solitary waves admitted by Eqs. (26)-(27), we consider points $C$ and $D$ in Fig. 3, where $\gamma = 0$. We look for the third reduction discussed above, i.e., $A_1 > 0$, $A_2 = i\hat{A}_2$, $\hat{A}_2 > 0$. In this case, the envelope solutions $A_1$ and $\hat{A}_2$ near points C and D with $\epsilon = 0.2$ are displayed in Figs. 5 and 6 respectively. At point $C$, $\sigma = 1$ (focusing nonlinearity), and $\eta = -1$; while at point $D$, $\sigma = -1$ (defocusing nonlinearity), and $\eta = 1$.

It should be noted that even though the envelope equations (26)-(27) are translation-invariant along the $X$ and $Y$ directions, the original equation (4) does

not allow that invariance due to the potential term. Hence envelopes $A_1, A_2$ can not be placed arbitrarily relative to the periodic potential. In the 1D case, it has been shown that the envelope solution can only be placed at two special locations of the potential [12]. In the present 2D case, we can show that envelopes $(A_1, A_2)$ can only be placed at four special positions relative to the periodic potentials. Specifically, the centers of these envelopes must be at $(x, y) = (0, 0), (0, \pi/2), (\pi/2, 0)$ or $(\pi/2, \pi/2)$, hence four different solitary waves can be obtained. Of course, these center positions can also be shifted by multiple periods $\pi$ along either of the $x$ and $y$ directions, but the resulting solutions are equivalent to the four mentioned above.

When envelope solutions $(A_1, A_2)$ of Eqs. (26)-(27) are substituted into the perturbation series (12), solutions of the original system (4) will be analytically obtained. To illustrate, we take the envelope solutions displayed in Figs. 5 and 6 for points $C$ and $D$, and let them be centered at the origin $(x, y) = (0, 0)$. Substituting these envelopes into the expansion (12), the leading-order solutions of Eq. (4) near points $C$ and $D$ are displayed in Fig. 7. We see that these solutions have interesting amplitude and phase structures. These structures have many common features. First, the amplitude fields of both solutions are dominant along the $x$ and $y$ directions, forming a cross pattern. Second, at the center of each lattice, i.e. points $x = m\pi, y = n\pi$ with $m, n$ being integers, the amplitudes are zero in both cases. Around each lattice center, the phase increases or decreases by $2\pi$. Thus the solution around each lattice center has a vortex-cell structure. Because of this, we can call these solutions vortex-array solitons. Differences between these two solutions are also apparent. One difference is that, at point $D$, the whole field is divided into disconnected cells. But at point C, only the outer field seems divided into disconnected cells; the inner field is totally connected. Another difference is that, at point $D$, each cell is either a vortex ring or dipole. At point $C$, however, the cells look quite different.

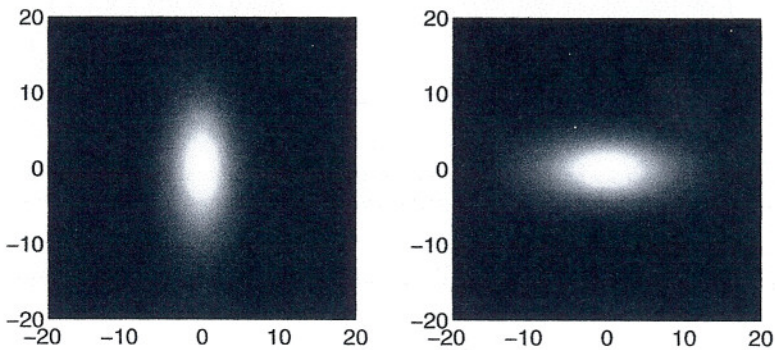


Figure 5. Envelop solutions $A_1$ (left) and $\hat{A}_2$ (right) near point $C$ with $\epsilon = 0.2$.

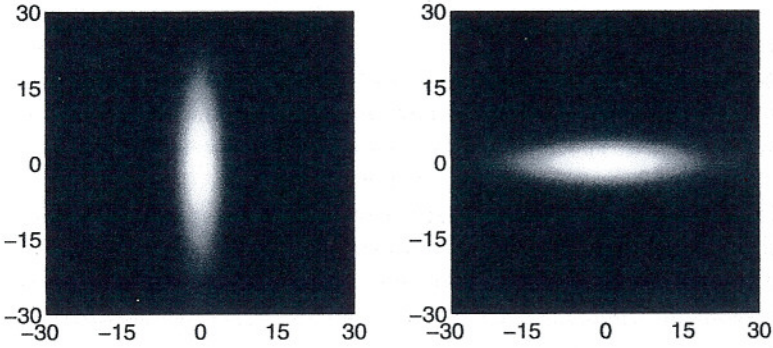


Figure 6. Envelop solutions $A_1$ (left) and $\hat{A}_2$ (right) near point $D$ with $\epsilon = 0.2$.

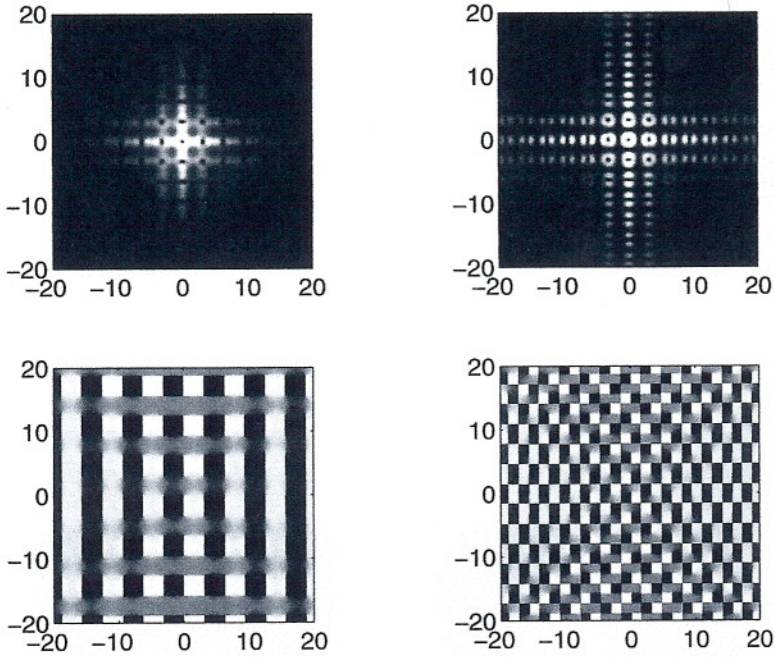


Figure 7. The leading-order analytical solutions near points $C$ (left column) and $D$ (right column) when $\epsilon = 0.2$. The top rows are amplitude plots, and the bottom rows are phase plots.

## 6. Numerical solutions of solitary waves at arbitrary amplitudes

The above multi-scale perturbation analysis is very valuable, as it clearly predicts various types of low-amplitude composite solitary waves near edges of Bloch bands. As the propagation constant $\mu$ moves away from these band edges, these solutions become more localized, and their amplitudes become higher. In such cases, the perturbation analysis starts to break down, and solutions need to be computed

numerically. In this section, we numerically determine whole families of composite solitary-wave solutions bifurcating from edges of Bloch bands. The numerical method we use is the modified squared-operator iteration method described in [20]. In these numerical computations, the above analytical solutions from the perturbation analysis are very important, as they are the starting point of our iteration scheme.

For illustration purpose, we present the families of solutions bifurcating from the vortex-array solitons of Fig. 7. The power curves of these solution families are shown in Fig. 8. Both curves have a power threshold, below which the solutions do not exist. As $\mu$ approaches the band edges, the powers of the $C$-family (left) and $D$-family (right) approach 10.4254 and 19.5470 respectively. Two solutions on each family (marked in the power curves of Fig. 8) are displayed in Figs. 9 and 10. In both figures, the left solution is close to the band edge, while the right solution is deep inside the band gap. As expected, when the solution is close to the band edge, its amplitude is low, and it is similar to the analytical solution shown in Fig. 7. This is a partial confirmation of our asymptotic analysis in the previous section. Deep inside the band gap, however, the solutions are very localized, and their profiles look quite different from the low-amplitude solutions. The features of these localized solutions can not be gleamed entirely from the analytical solutions, thus their numerical computations are necessary and helpful. The vortex-array soliton in the right column of Fig. 9 corresponds to the higher-band vortex observed in [17] (where nonlinearity is of focusing type). The vortex-array soliton in the right column of Fig. 10 for defocusing nonlinearity has never been reported before in the literature.

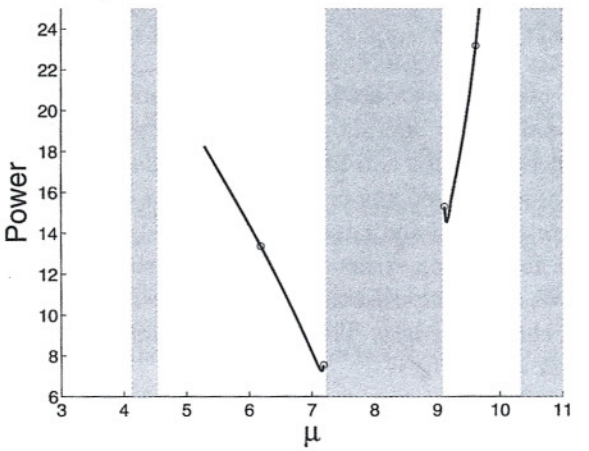


Figure 8. Power curves of composite vortex-array solitons bifurcating from points $C$ (left) and $D$ (right) of Fig. 3. The circle points are where we plot the numerical solutions in the following figures. In the left band gap, the circle points are 1.04 and 0.04 from the band edge. In the right band gap, the circle points are 0.54 and 0.04 from the band edge.

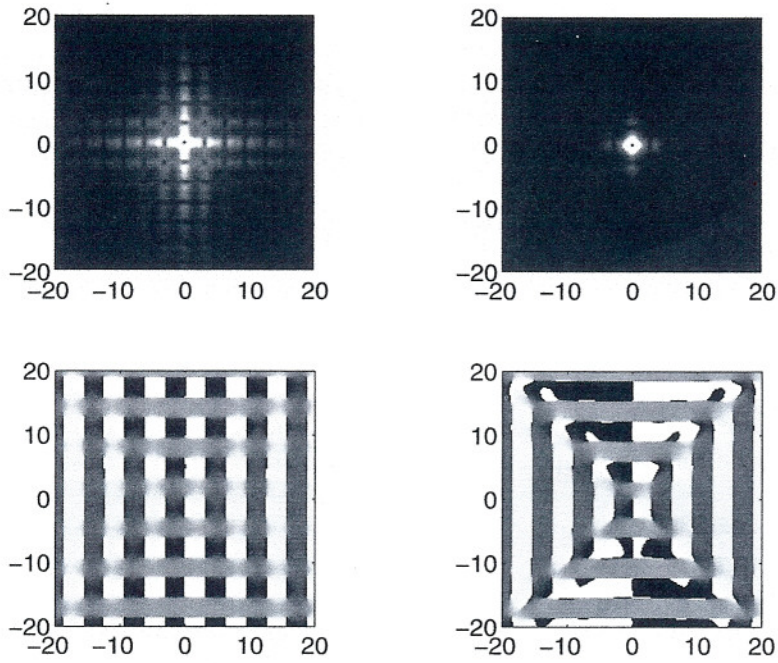


Figure 9. The amplitude (top) and phase (bottom) structures of two vortex-array solitons bifurcating from point C of Fig. 3 for focusing nonlinearity. The propagation constants of these two solutions are 7.1891 (left) and 6.1891 (right), as marked in Fig. 8.

## 7. Conclusion

In this paper, we obtained new solitary-wave structures in two-dimensional periodic media both analytically and numerically. These new structures bifurcate from the edges of Bloch bands with two linearly independent Bloch modes. Using perturbation methods, we derived the coupled nonlinear envelope equations for these composite solitons near the band edges. These envelope equations admit solutions which give rise to new soliton structures such as vortex-array solitons. Using numerical methods, we also computed these composite solitons directly both near and further away from the band edges. The numerical results are in full agreement with analytical ones near band edges.

## Acknowledgments

This work was partially supported by the U.S. Air Force Office of Scientific Research under grant USAF 9550-05-1-0379.

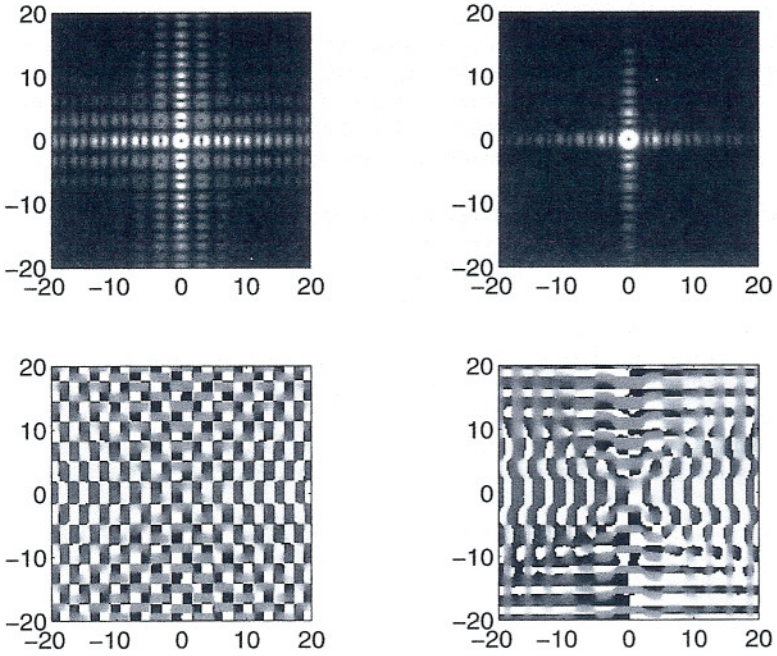


Figure 10. The amplitude (top) and phase (bottom) structures of two vortex-array solitons bifurcating from point D of Fig. 3 for defocusing nonlinearity. The propagation constants of these two solutions are 9.1210 (left) and 9.6210 (right), as marked in Fig. 8.

## References


1. J.D. Joannopoulos, R.D. Meade, and J.N. Winn, *Photonic Crystals: Molding the Flow of Light*, Princeton University Press, 1995.
2. P. Russell, "Photonic Crystal Fibers", Science, 299, pp. 358 - 362 (2003).
3. H. S. Eisenberg, Y. Silberberg, R. Morandotti, A. R. Boyd, and J. S. Aitchison, Discrete Spatial Optical Solitons in Waveguide Arrays, Phys. Rev. Lett. 81, 3383-3386 (1998).
4. J.W Fleischer, M. Segev, N.K Efremidis, and D.N Christodoulides, "Observation of two-dimensional discrete solitons in optically induced nonlinear photonic lattices", Nature 422, 147 (2003).
5. H. Martin, E.D. Eugenieva, Z. Chen and D.N. Christodoulides, Discrete solitons and soliton-induced dislocations in partially-coherent photonic lattices, Phys. Rev. Lett. 92, 123902 (2004).
6. R. Iwanow, R. Schiek, G. I. Stegeman, T. Pertsch, F. Lederer, Y. Min, and W. Sohler, Observation of Discrete Quadratic Solitons, Phys. Rev. Lett. 93, 113902( 2004).
7. F. Fedele, J. Yang, and Z. Chen, "Defect modes in one-dimensional photonic latices." Opt. Lett. 30, 1506 (2005).
8. I. Makasyuk, Z. Chen and J. Yang, "Bandgap guidance in optically-induced photonic lattices with a negative defect", Phys. Rev. Lett. 96, 223903 (2006).
9. F. Dalfovo, S. Giorgini, L. P. Pitaevskii, and S. Stringari, "Theory of Bose-Einstein condensation in trapped gases", Rev. Mod. Phys. 71, 463 (1999).
10. J.W. Fleischer, T. Carmon, M. Segev, N.K. Efremidis, and D.N. Christodoulides, Observation of Discrete Solitons in Optically Induced Real Time Waveguide Arrays,

Phys. Rev. Lett. 90, 023902 (2003).
11. D. Neshev, E. Ostrovskaya, Yu.S. Kivshar, W. Krolikowski, Spatial solitons in optically induced gratings, Opt. Lett. 28, 710 (2003).
12. D. E. Pelinovsky, A. A. Sukhorukov, and Y. S. Kivshar, "Bifurcations and stability of gap solitons in periodic potentials", Phys. Rev. E 70, 036618 (2004).
13. B. A. Malomed and P. G. Kevrekidis, Discrete vortex solitons, Phys. Rev. E 64, 026601 (2001).
14. J. Yang and Z.H. Musslimani, Fundamental and vortex solitons in a two-dimensional optical lattice. Opt. Lett. 23, 2094 (2003).
15. D.N. Neshev, T.J. Alexander, E.A. Ostrovskaya, Y.S. Kivshar, H. Martin, Z. Chen, Observation of Discrete Vortex Solitons in Optically Induced Photonic Lattices. Phys. Rev. Lett. 92, 123903 (2004).
16. J.W. Fleischer, G. Bartal, O. Cohen, O. Manela, M. Segev, J. Hudock, D.N. Christodoulides, Observation of vortex-ring discrete solitons in 2D photonic lattices. Phys. Rev. Lett. 92, 123904 (2004).
17. G. Bartal, O. Manela, O. Cohen, J.W. Fleischer, and M. Segev, "Observation of Second-Band Vortex Solitons in 2D Photonic Lattices", Phys. Rev. Lett. 95, 053904 (2005).
18. I. Makasyuk, Z. Chen and J. Yang, "Bandgap guidance in optically-induced photonic lattices with a negative defect", Phys. Rev. Lett. 96, 223903 (2006).
19. J. Yang, Stability of vortex solitons in a photorefractive optical lattice. New Journal of Physics 6, 47 (2004).
20. J. Yang and T.I. Lakoba, "Squared-operator iteration methods for solitary waves in general nonlinear wave equations." To appear in Stud. Appl. Math.